SLAC-PUB-8748
BABAR-PROC-00/34
hep-ex/0101004
September, 2000

The first physics results from BaBar.

G. Sciolla
Stanford Linear Accelerator Center
Mail Stop 95, P.O. Box 4339, Stanford, CA 94309, USA
(for the *BABAR* Collaboration)

Abstract

The BABAR experiment and the PEP-II accelerator at SLAC started to take data on May 26, 1999. By the time of this conference, the recorded integrated luminosity was 20 fb^{-1}, of which 8 fb^{-1} were analyzed to provide a first set of physics results. This talk reviews the first measurement of $\sin 2\beta$ and the study of B meson decays to charmonium modes and 2-body charmless decays. Complementary results were presented by the BABAR Collaboration at this conference and are reviewed in [1].

Contribued to the Proceedings of the International Conference On CP Violation Physics,
18-22 Sep 2000, Ferrara, Italy

Stanford Linear Accelerator Center, Stanford University, Stanford, CA 94309

Work supported in part by Department of Energy contract DE-AC03-76SF00515.

1 Physics at *BABAR*

The BABAR experiment [2] is designed in order to perform a comprehensive study of CP violation in the B system. The main goal is to investigate if CP violation can be fully explained within the Standard Model by the imaginary phase of the Cabibbo-Kobayashi-Maskawa matrix, or if other sources of CP violation should be looked for elsewhere [3].

The strategy is to over-constrain the Unitarity Triangle by measuring at the same time its sides and angles.

The sides can be extracted from measurements of $|V_{tb}^* V_{td}|$ in the study of $B^0\overline{B}^0$ mixing, V_{ub} from the study of decays of B mesons in charmless final states, and V_{cb} from studies of the decay $B \to D^* l\nu$.

The determination of the angles requires to measure time dependent asymmetries for the decay of a neutral B meson into a CP eigenstate, f_{CP}, of the form

$$\mathcal{A}_{CP}(t) = \frac{\Gamma(B^0(t) \to f_{CP}) - \Gamma(\overline{B^0}(t) \to f_{CP})}{\Gamma(B^0(t) \to f_{CP}) + \Gamma(\overline{B^0}(t) \to f_{CP})}. \quad (1)$$

For B^0 decays with only one diagram contributing to the final state

$$\mathcal{A}_{CP}(t) = -\mathrm{Im}\lambda \sin(\Delta m \Delta t), \quad (2)$$

where $\lambda = p/q\overline{A}(f)/A(f)$, $A(f)$ and $\overline{A}(f)$ are the decay amplitudes and p and q are the complex coefficients that relate mass and flavour eigenstates of the B mesons [3]. For some decay modes, $\mathrm{Im}\lambda$ is directly and simply related to the angles of the Unitarity Triangle. Of particular interest are the decays of the neutral B mesons in final states containing a charmonium state and a neutral kaon. For these decays

$$\mathcal{A}_{CP}(t) = \pm \sin(2\beta) \sin(\Delta m \Delta t). \quad (3)$$

Experimentally, the measurement of the CP asymmetry $\mathcal{A}_{CP}$ requires three basic steps:

- the exclusive reconstruction of one B meson (B_{CP}) in a CP eigenstate (e.g. $B^0 \to J/\psi K_s$);
- the measurement of the time Δt elapsed between the decay of the two neutral B mesons produced in the $\Upsilon(4S)$ decay;
- the tagging of the CP eigenstate at the production time, inferred from the tagging of the other B meson (B_{tag}) produced coherently in the $\Upsilon(4S)$ decay.

2 The experimental apparatus

The PEP-II storage ring and the BABAR detector have been designed specifically to measure time-dependent CP asymmetries in the neutral B meson decays in the most effective way.

2.1 The PEP-II accelerator

PEP-II is an asymmetric B factory consisting of two concentric rings: a high energy ring (HER) with a 9.0 GeV electron beam and a low energy ring (LER) with a 3.1 GeV positron beam. The energy of the two beams has been chosen in order to achieve a center of mass energy of 10.58 GeV, the mass of the $\Upsilon(4S)$ resonance, and a boost of 0.56 of the $\Upsilon(4S)$ along the z axis. The boost

Table 1: Typical reconstruction efficiencies and pion misidentification probabilities for electrons, muons and kaons in BABAR.

Particle	Efficiency	π contamination
electrons	92%	0.3%
muons	75%	2.5%
kaons	85%	5%

corresponds to an average separation of 260 μm between the decay vertices of the two B mesons produced in the $\Upsilon(4S)$ decay. The design luminosity of the machine is $3\times10^{33}s^{-1}cm^{-2}$, which corresponds to about 30 million $B\overline{B}$ pairs produced per year.

PEP-II started its activity in factory mode on May 26, 1999 and reached outstanding performance very rapidly. By the time of this conference the achieved peak luminosity was 2.56 $\times10^{33}s^{-1}cm^{-2}$, which corresponds to 85% of the design value. The design daily recorded luminosity of 135 pb^{-1}/day was routinely achieved and exceeded starting in June 2000, with a record of 151 pb^{-1} accumulated in one day. By the time of this conference the total integrated luminosity delivered by PEP-II was 19.5 fb^{-1}, of which 17.5 recorded at the $\Upsilon(4S)$ resonance and 2 fb^{-1} at a center of mass about 40 MeV below resonance. Thanks to a data taking efficiency higher than 95%, BABAR accumulated more than 18 fb^{-1} on tape.

2.2 The *BABAR* detector

BABAR is a cylindrical detector built around the interaction point of PEP-II. It consists of several concentric subdetectors. From the inside out there are:

- a silicon vertex tracker, consisting of 5 layers of double-sided silicon strips;
- a cylindrical drift chamber, filled with a low density gas mixture (Helium-Isobutane: 80%-20%) to minimize multiple scattering;
- the DIRC detector, the main particle identification device of the experiment, which consists of 144 quartz bars;
- an electromagnetic calorimeter, consisting of 6580 CsI crystals;
- a 1.5 Tesla superconducting magnet;
- an instrumented flux return (IFR), consisting of 19 layers of RPCs, for muon identification and K_L reconstruction.

The combined tracking resolution of the BABAR experiment can be parameterized as

$$\left(\frac{\Delta p_T}{p_T}\right)^2 = (0.0015 p_T)^2 + 0.005^2. \quad (4)$$

The performances of electron, muon and kaon identification are summarized in Table 1. Of particular interest is the good kaon-pion separation capability of the detector obtained from the measurement of the Cherenkov angle by the DIRC detector. The separation is better than 3σ up to momenta of 3.5 GeV/c as illustrated in Figure 1.

A more detailed description of detector design and performance can be found in [4].

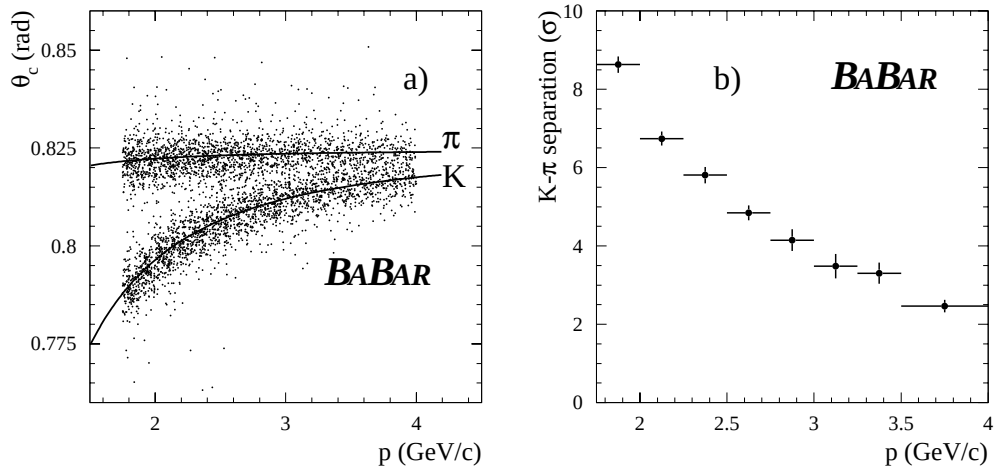

Figure 1: (a) The Cherenkov angle and (b) K–π separation as functions of momentum for single tracks in a D^0 control sample. The separation is an average over all polar angles.

2.3 The data set

Unless otherwise specified, all the results presented in this talk are based on a data set of 7.7 fb^{-1} recorded at the $\Upsilon(4S)$ resonance and 1.2 fb^{-1} recorded off peak. These data were recorded by the BABAR detector between January and June 2000.

Since the analyses are still in progress, all results are preliminary.

3 Study of B $\to$ charmonium decays

A good understanding of B meson decays into final states containing a charmonium resonance is a prerequisite to an analysis of CP violation in the B system. In this section, an extensive set of measurements of inclusive and exclusive branching fractions of B mesons into charmonium decays is briefly summarized. More details can be found in [5] and [6].

3.1 Inclusive analysis

J/ψ candidates are formed from pairs of oppositely charged tracks both identified as leptons. Figure 2 shows the invariant mass distributions for $J/\psi \to e^+e^-$ and $J/\psi \to \mu^+\mu^-$ candidates after continuum subtraction. The number of J/ψ mesons is extracted from the mass distribution using a probability density function (p.d.f.) derived from a simulation that includes final state radiation and bremsstrahlung. A total of $4920 \pm 100 \pm 180$ $J/\psi \to e^+e^-$ and $5490 \pm 90 \pm 90$ $J/\psi \to \mu^+\mu^-$ events were reconstructed.

The $\psi(2S)$ was reconstructed in its decays to e^+e^-, $\mu^+\mu^-$ and $J/\psi\,\pi^+\pi^-$. For the modes $\mu^+\mu^-$ and e^+e^-, the numbers of signal events are extracted from the mass distribution using a p.d.f. from simulation. A total of 131 ± 29 $\psi(2S) \to e^+e^-$ and 125 ± 19 $\psi(2S) \to \mu^+\mu^-$ events were found. For the decays $J/\psi\,\pi^+\pi^-$, the yields are extracted from a fit to the distribution of the mass difference between the $\psi(2S)$ and the J/ψ in order to reduce the impact of the radiative tail and

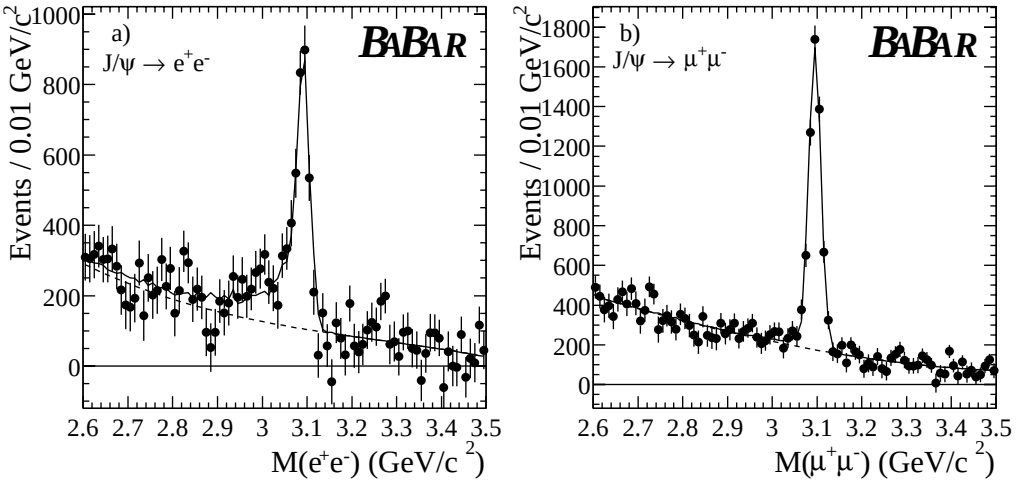

Figure 2: Mass distribution of J/ψ candidates to (a) electron pairs and (b) muon pairs after the continuum subtraction.

the mass resolution of the J/ψ candidate. A total of 126 ± 44 events were found in candidates with $J/\psi \to e^+e^-$, and 162 ± 23 events for $J/\psi \to \mu^+\mu^-$.

χ_c mesons are reconstructed through the radiative decay $\chi_c \to \gamma J/\psi$. The selected photon candidates must have an energy between 0.20 and 0.65 GeV in the CM system and be isolated from nearby hadronic showers. The substantial combinatorial background from π^0 decays is reduced by rejecting any photon that, when combined with any other photon, gives an invariant mass compatible with a π^0.

As for the $\psi(2S)$, the numbers of events are extracted by fitting the distribution of the mass difference between the χ_c and J/ψ candidates (Figure 3). We simultaneously fit for a χ_{c1} and a possible χ_{c2} component, assuming the resolution of the two resonances to be the same and fixing the difference between the χ_{c2} and the χ_{c1} masses to the Particle Data Group value. We found $129 \pm 26 \pm 13$ χ_{c1} and 3 ± 21 χ_{c2} events in which J/ψ decayed into e^+e^-, and $204 \pm 47 \pm 12$ χ_{c1} and 47 ± 21 χ_{c2} events for the $\mu^+\mu^-$ mode.

Due to the preliminary status of the analysis, we chose not to quote a branching ratio for B $\to$ J/ψ X at this time. The yields obtained for the decay B $\to$ J/ψ X are used, together with the already precise value of the branching fraction for this decay reported in [7], as a normalization in the calculation of the branching ratios of $B \to \psi(2s)X$ and $B \to \chi_c X$. The results, summarized in Table 2, are very competitive compared with the world averages.

3.2 Exclusive analysis

We considered the exclusive B decay channels listed in Table 3.

In these analyses, the reconstruction of the charmonium decays is very similar to the one used for inclusive analysis, but with looser requirements for the lepton identification. In the case of the decay $J/\psi \to e^+e^-$, we apply a procedure to add photons which are close to the electron tracks in order to reduce the impact of bremsstrahlung on the reconstruction efficiency.

$K^0_S \to \pi^+\pi^-$ candidates are formed from pairs of oppositely charged tracks which have an invariant mass between 0.489 and 0.507 GeV/c^2. In addition we require that the K^0_S be consistent

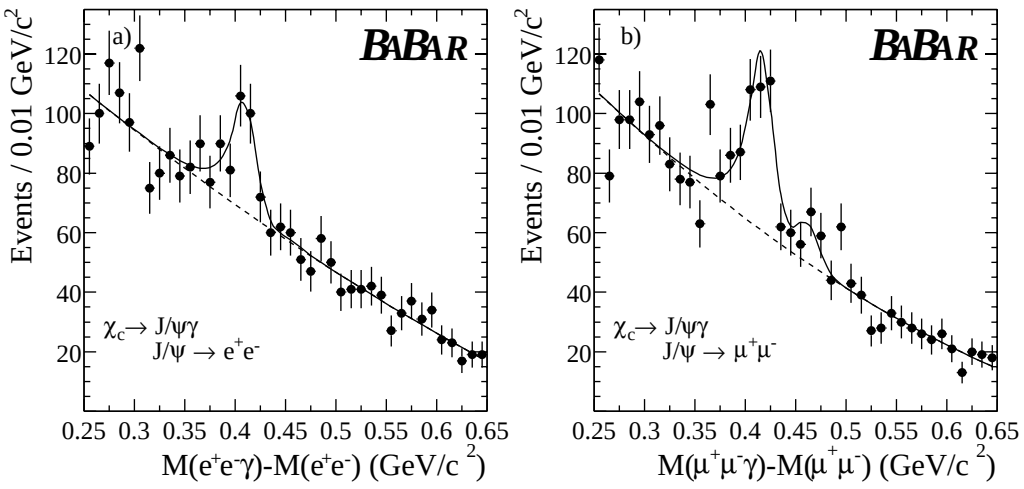

Figure 3: Mass difference between the χ_c and J/ψ candidates, where $\chi_c \to \gamma J/\psi$ and (a) $J/\psi \to e^+e^-$ and (b) $J/\psi \to \mu^+\mu^-$.

Table 2: Summary of inclusive B branching ratios measured with respect to $B \to J/\psi X$. The results are combined and multiplied by the PDG value for $\mathcal{B}(B \to J/\psi X)$ to obtain inclusive branching fractions (%).

	Branching ratio relative to $J/\psi X$							Branching fraction (%)		
	e^+e^-			$\mu^+\mu^-$			Common	Combined		
		Stat	Sys		Stat	Sys	Sys (%)		Stat	Sys
$\chi_{c1} \to \gamma J/\psi$	0.28	$\pm$ 0.06	$\pm$0.03	0.38	$\pm$0.05	$\pm$0.02	$\pm$7.3	0.39	$\pm$0.04	$\pm$0.04
χ_{c2} 90% CL	< 0.16			< 0.28			$\pm$8.1	< 0.24		
$\psi(2S) \to \ell^+\ell^-$	0.22	$\pm$0.05	$\pm$0.01	0.23	$\pm$0.04	$\pm$0.01	$\pm$13.6	0.26	$\pm$0.03	$\pm$0.04
$\psi(2S) \to \pi\pi J/\psi$	0.18	$\pm$0.06	$\pm$0.01	0.22	$\pm$0.03	$\pm$0.00	$\pm$9.9	0.24	$\pm$0.03	$\pm$0.03
Combined $\psi(2S)$								0.25	$\pm$0.02	$\pm$0.02

with having originated from the J/ψ vertex.

$K^0_S \to \pi^0\pi^0$ candidates are required to have a mass between 0.470 and 0.525 GeV/c^2 and an energy greater than 0.8 GeV. A π^0 decay to two photons is observed in the EMC either as a single neutral cluster with substructure or as two distinct γ clusters. The most probable decay point of the K^0_S is determined after refitting the two π^0 mesons at several points along the path defined by their summed momentum vector and the J/ψ vertex.

We reconstruct K^{*0} decays to $K^+\pi^-$ and $K^0_S\pi^0$, and K^{*+} decays to $K^0_S\pi^+$ and $K^+\pi^0$. In all cases the candidate K^* is required to have an invariant mass within 0.075 GeV/c^2 of the nominal value.

Charged kaons are identified by the Cherenkov angle measured by the DIRC detector and/or by the specific ionization measurement (dE/dx) in the DCH, depending on particle momentum.

To isolate the signal for each mode we use the variables ΔE, the difference between the reconstructed and expected B meson energy measured in the center-of-mass frame, and $m_{\rm ES}$, the beam-energy substituted mass. These variables are defined as:

$$m_{\rm ES} = \sqrt{E^{*2}_b - \boldsymbol{p}^{*2}_B}, \quad (5)$$

$$\Delta E = E^*_B - E^*_b, \quad (6)$$

where E^*_b is the beam energy in the center-of-mass, and E^*_B and $\boldsymbol{p}^*_B$ are the energy and momentum of the reconstructed B meson in the center-of-mass.

When deriving branching fractions we have used the secondary branching fractions and their associated errors published by the Particle Data Group [7].

We determine the number of $B\overline{B}$ events from the difference in the multi-hadron rates on and off the $\Upsilon(4S)$ resonance, normalized to the respective luminosities. The efficiencies for each mode have been obtained from Monte Carlo simulations complemented with measurements of tracking and particle identification efficiencies extracted from data. The shape of the beam-energy substituted mass distribution is parameterized for each mode with the sum of a Gaussian and the ARGUS function [8].

Figure 4 shows the $m_{\rm ES}$ and ΔE distributions of the candidates. In Table 4 we present the yields and measured branching fractions for the individual exclusive modes. Figure 5 shows the measured branching fractions compared to the values compiled by the Particle Data Group [7].

Table 3: Exclusive B meson decay modes.

Channel	Secondary decay mode(s)
$B^0 \to J/\psi\, K^0_S$	$J/\psi \to \ell^+\ell^-$
	$K^0_S \to \pi\pi,\ \pi^0\pi^0$
$B^+ \to J/\psi\, K^+$	$J/\psi \to \ell^+\ell^-$
$B^0 \to J/\psi\, K^{*0}$	$J/\psi \to \ell^+\ell^-$
	$K^{*0} \to K^+\pi^-,\ K^0_S\pi^0$
$B^+ \to J/\psi\, K^{*+}$	$J/\psi \to \ell^+\ell^-$
	$K^* \to K^0_S\pi^-,\ K^+\pi^0$
$B^0 \to \psi(2S) K^0_S$	$\psi(2S) \to \ell^+\ell^-,\ J/\psi\,\pi\pi$
	$K^0_S \to \pi\pi$
$B^+ \to \psi(2S) K^+$	$\psi(2S) \to \ell^+\ell^-,\ J/\psi\,\pi\pi$
$B^+ \to \chi_{c1} K^+$	$\chi_{c1} \to J/\psi\gamma;\ J/\psi \to \ell^+\ell^-$

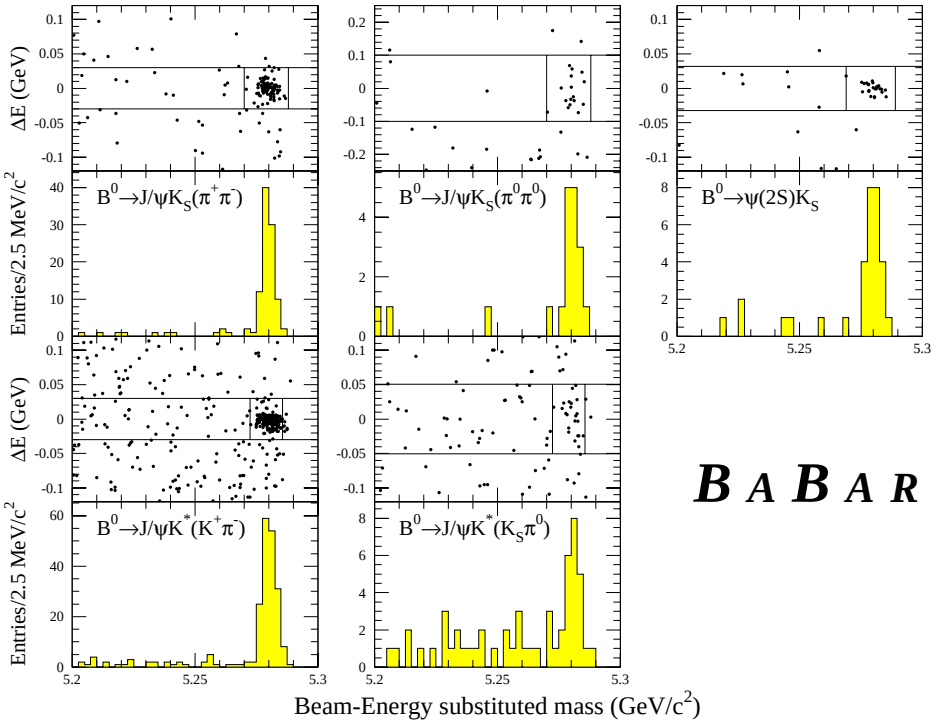

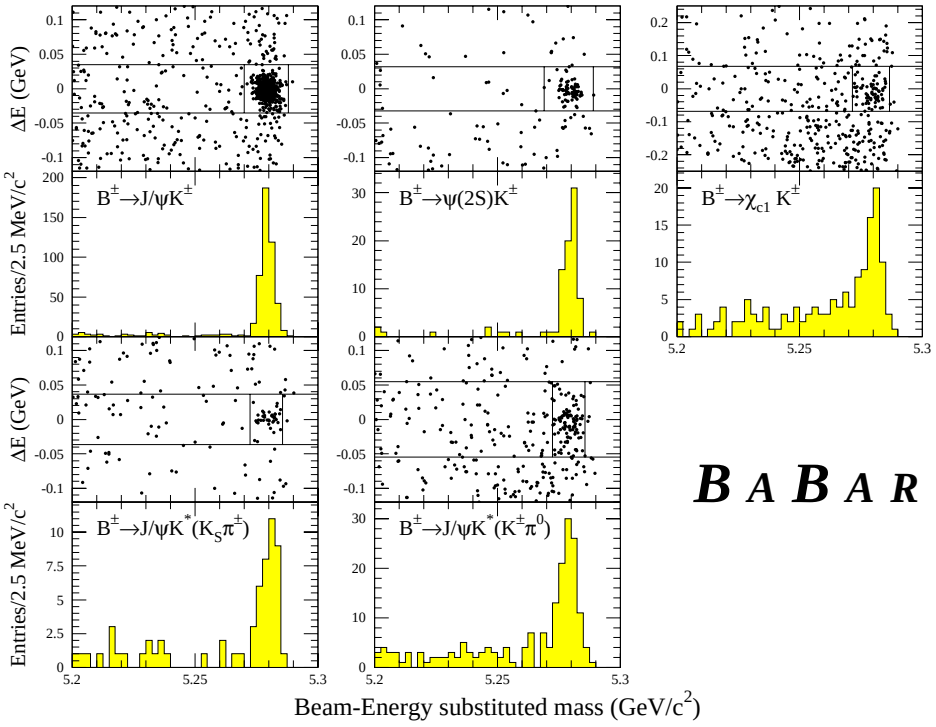

Figure 4: Distributions of candidate events in $m_{\rm ES}$ and ΔE. The upper plot shows the B^0 modes and the lower plot the B^+ modes.

Table 4: The yields and measured branching fractions for exclusive decays of B mesons involving charmonium. The errors on the yields are only statistical. For the branching fractions, the first error is statistical and the second systematic.

Channel	Yield	Br. Frac./10^{-4}
$B^0 \to J/\psi K^0$		
$K^0_S \to \pi^+\pi^-$	93 ± 10	$10.2 \pm 1.1 \pm 1.3$
$K^0_S \to \pi^0\pi^0$	14 ± 4	$7.5 \pm 2.0 \pm 1.2$
$B^+ \to J/\psi K^+$	445 ± 21	$11.2 \pm 0.5 \pm 1.1$
$B^0 \to J/\psi K^{*0}$	188 ± 14	$13.8 \pm 1.1 \pm 1.8$
$B^+ \to J/\psi K^{*+}$	126 ± 12	$13.2 \pm 1.4 \pm 2.1$
$B^0 \to \psi(2S) K^0$	23 ± 5	$8.8 \pm 1.9 \pm 1.8$
$B^+ \to \psi(2S) K^+$	73 ± 8	$6.3 \pm 0.7 \pm 1.2$
$B^+ \to \chi_{c1} K^+$	44 ± 9	$7.7 \pm 1.6 \pm 0.9$

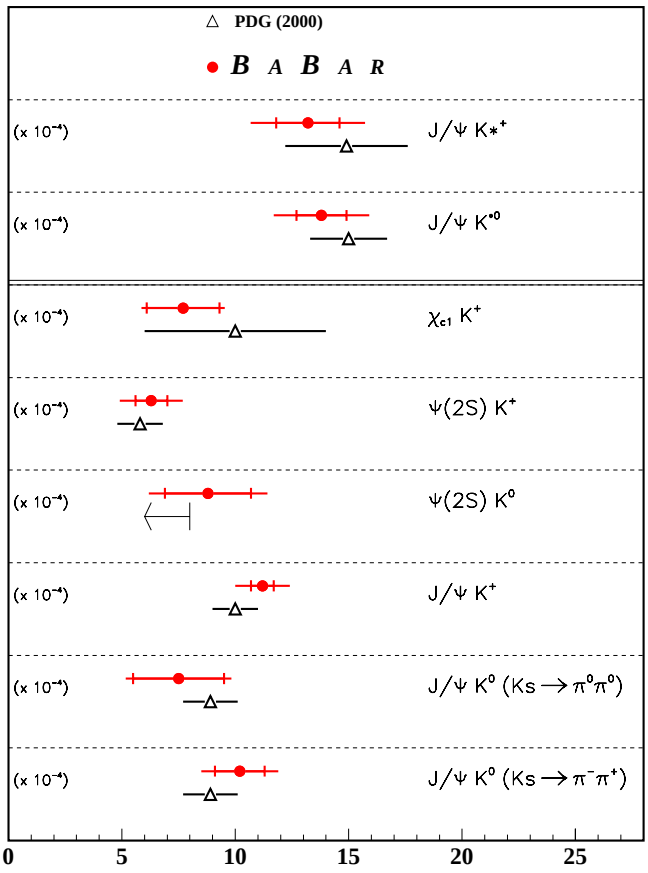

Figure 5: Summary of branching fraction measurements for charmonium + K channels and comparisons with the PDG 2000 values.

4 Measurement of $\sin 2\beta$

The measurement of sin2β requires five basic steps: exclusive reconstruction of the CP mode; measurement of time elapsed between the decays of the two B mesons; tagging of the flavour of the B meson at production time; measurement of the dilution factors from the data; extraction of the value of sin2β from a fit to the amplitude of the *CP* asymmetry. The following subsections briefly describe the analysis strategy and the result. For a more detailed description see [9] and references therein.

4.1 Reconstruciton of the CP mode

For a first measurement, we targeted only decays characterized by relatively high accessible branching fractions ($\sim 10^{-4}$–10^{-5}), low backgrounds (<10%), and reliable theoretical prediction (i.e., no penguin pollution). Only the decays $B \to J/\psi K_s$ and $B \to \psi(2S)K_s$ have been used so far. The procedure used for the exclusive reconstruction of the B meson is described in [6].

The yields and purities obtained in each channel analysing 9 fb^{-1} are reported in Table 5. The modes $B \to \chi_c K_s$, $B \to J/\psi K_L$ and $B \to J/\psi K^{*0}$ are still under investigation and will be included in the analysis in the future.

4.2 Time resolution function

The resolution of the Δt measurement is dominated by the z resolution of the tagging vertex. The three-momentum of the tagging B and its associated error matrix are derived from the fully reconstructed B_{CP} candidate three momentum, decay vertex and error matrix, and from the knowledge of the average position of the interaction point and the $\Upsilon(4S)$ four-momentum. This derived B_{tag} three-momentum is fit to a common vertex with the remaining tracks in the event (excluding those from B_{CP}). In order to reduce the bias due to long-lived particles, all reconstructed V^0 candidates are used as input to the fit in place of their daughters. Any track whose contribution to the χ^2 is greater than 6 is removed from the fit. This procedure is iterated until there are no tracks contributing more than 6 to the χ^2 or until all tracks are removed.

The time resolution function is described by the sum of two Gaussian distributions:

$$\mathcal{R}(\Delta t) = \sum_{i=1}^{2} \frac{f_i}{\sigma_i \sqrt{2\pi}} \exp\left(-\frac{(\Delta t - \delta_i)^2}{2{\sigma_i}^2}\right). \tag{7}$$

Monte Carlo simulation indicates that 70% of the events are in the core Gaussian, which has a width $\sigma_1 \approx 0.6$ ps. The wide Gaussian has a width $\sigma_2 \approx 1.8$ ps. Tracks from forward-going charm decays included in the reconstruction of the B_{tag} vertex introduce a small bias, $\delta_1 \approx -0.2$ ps, for the core Gaussian.

Table 5: The CP sample used for the sin2β measurement: yields and purities obtained using 9 fb^{-1}.

Decay mode	Yield	Purity
$J/\psi K_s(K_s \to \pi^+\pi^-)$	124 ± 12	96%
$J/\psi K_s(K_s \to \pi^0\pi^0)$	18 ± 4	91%
$\psi(2s)K_s(K_s \to \pi^+\pi^-)$	27 ± 6	93%

Table 6: Parameters of the resolution function determined from the sample of events with fully-reconstructed hadronic B^0 candidates.

Parameter		Value	
δ_1	(ps)	-0.20 ± 0.06	from fit
$\mathcal{S}_1$		1.33 ± 0.14	from fit
f_w	(%)	1.6 ± 0.6	from fit
f_1	(%)	75	fixed
δ_2	(ps)	0	fixed
$\mathcal{S}_2$		2.1	fixed

A small fraction of events ($\sim$1%) have very large values of Δz, mostly due to vertex reconstruction problems. This is accounted for in the parameterization of the time resolution function with a very wide unbiased Gaussian with fixed width of 8 ps.

In likelihood fits, we use a parameterization of the error $\sigma_{\Delta t}$ calculated from the fits to the two B vertices for each individual event. We introduce two scale factors $\mathcal{S}_1$ and $\mathcal{S}_2$ for the width of the narrow and the wide Gaussian distributions ($\sigma_1 = \mathcal{S}_1 \times \sigma_{\Delta t}$ and $\sigma_2 = \mathcal{S}_2 \times \sigma_{\Delta t}$) to account for the fact that the uncertainty on Δt is underestimated due to effects such as the inclusion of particles from D decays and possible underestimation of the amount of material traversed by the particles. The scale factor $\mathcal{S}_1$ and the bias δ_1 of the narrow Gaussian are free parameters in the fit. The scale factor $\mathcal{S}_2$ and the fraction of events in the wide Gaussian, f_2, are fixed to the values estimated from Monte Carlo simulation by a fit to the pull distribution ($\mathcal{S}_2 = 2.1$ and $f_2 = 0.25$). The bias of the wide Gaussian, δ_2, is fixed at 0 ps. The last free parameter in the fit is f_w, the fraction of the very wide Gaussian that describes the tail of the resolution.

Because the time resolution is dominated by the precision of the B_{tag} vertex position, we find no significant differences in the Monte Carlo simulation of the resolution function parameters for the various fully reconstructed decay modes. This allows us to determine the resolution function parameters with the relatively high-statistics fully-reconstructed B^0 data samples. The differences in the resolution function parameters in the different tagging categories (see below) are also small.

Table 6 presents the values of the Δt resolution parameters obtained from a maximum likelihood fit to a sample of fully reconstructed B^0 decays. Further details on the procedure and the results can be found in [10]. The vertex parameters are fixed to these values in the final unbinned maximum likelihood fit for sin2β in the low-statistics *CP* event sample.

4.3 B flavor tagging

Each event with a *CP* candidate is assigned a B^0 or $\overline{B}^0$ tag if the rest of the event (i.e., with the daughter tracks of the B_{CP} removed) satisfies the criteria for one of several tagging categories. The figure of merit for each tagging category is the effective tagging efficiency $Q_i = \varepsilon_i\ (1 - 2w_i)^2$, where ε_i is the fraction of events assigned to category i and w_i is the probability of misclassifying the tag as a B^0 or $\overline{B}^0$ for that category. w_i are called mistag fractions. The statistical error on sin2β is proportional to $1/\sqrt{Q}$, where $Q = \sum_i Q_i$.

The algorithm used in the analysis categorizes the events in four different classes:

`Lepton` when the flavor of the B meson is identified by the charge of the high momentum lepton coming from a semileptonic decay;

Table 7: Categories of tagged events in the *CP* sample. The `Lepton` category is split into `Electron` and `Muon` categories.

Tagging Category	$J/\psi K^0_S$						$\psi(2S)K^0_S$			*CP* sample		
	$(K^0_S \to \pi^+\pi^-)$			$(K^0_S \to \pi^0\pi^0)$			$(K^0_S \to \pi^+\pi^-)$			(tagged)		
	B^0	$\overline{B}^0$	all	B^0	$\overline{B}^0$	all	B^0	$\overline{B}^0$	all	B^0	$\overline{B}^0$	all
`Electron`	1	3	4	1	0	1	1	2	3	3	5	8
`Muon`	1	3	4	0	0	0	2	0	2	3	3	6
`Kaon`	29	18	47	2	2	4	5	7	12	36	27	63
`NT1`	9	2	11	1	0	1	2	0	2	12	2	14
`NT2`	10	9	19	3	3	6	3	1	4	16	13	29
`Total`	50	35	85	7	5	12	13	10	23	70	50	**120**

`Kaon` when the flavor of the B meson is identified by the charge of the kaon coming from the hadronization of the s quark coming from the decay $b \to c \to s$;

`NT1` the tag is chosen according to the output of a neural network that exploits other (correlated) information, such as secondary lepton charge, slow pions from D^* decays, jet charge;

`NT2` similar to NT1 but characterized by a smaller tagging power.

When an event satisfied the selection criteria for more than one tagging category, it was assigned to the tag with the highest discrimination power.

4.3.1 Measurement of mistag fractions

The mistag fractions are measured directly in events in which one B^0 candidate, called the B_{rec}, is fully reconstructed in a flavor eigenstate mode. The flavor-tagging algorithms described in the previous section are applied to the rest of the event, which constitutes the potential B_{tag}.

Considering the $B^0\overline{B}^0$ system as a whole, one can classify the tagged events as *mixed* or *unmixed* depending on whether the B_{tag} is tagged with the same flavor as the B_{rec} or with the opposite flavor. The observed fraction of mixed events at the time t is expressed as

$$\chi(\Delta t) = w + D/2(1 - \cos(\Delta m \Delta t)), \tag{8}$$

were $D = 1 - 2w$ is the so called *dilution factor*. The mixing probability is smallest for small values of $\Delta t = t_{rec} - t_{tag}$ so that the apparent rate of mixed events near $\Delta t = 0$ is governed by the mistag probability. In addition to improving sensitivity to the mistag fraction, this time-dependent measurement technique also helps discriminate against backgrounds with different time-dependence.

The extraction of the mistag probabilities is complicated in reality by the possible presence of mode-dependent backgrounds. We deal with these by adding specific terms in the likelihood functions describing the different types of backgrounds (zero lifetime, non-zero lifetime without mixing, non-zero lifetime with mixing). Details are described in [1] and [10].

The mistag fractions and the tagging efficiencies obtained by combining the results from maximum likelihood fits to the time distributions in the B^0 hadronic and semileptonic samples are summarized in Table 8. We find a tagging efficiency of $(76.7 \pm 0.5)\%$ (statistical error only). The

Table 8: Mistag fractions measured from a maximum-likelihood fit to the time distribution for the fully-reconstructed B^0 sample. The uncertainties on ε and Q are statistical only.

Category	ε (%)	w (%)	Q (%)
`Lepton`	11.2 ± 0.5	$9.6 \pm 1.7 \pm 1.3$	7.3 ± 0.7
`Kaon`	36.7 ± 0.9	$19.7 \pm 1.3 \pm 1.1$	13.5 ± 1.2
`NT1`	11.7 ± 0.5	$16.7 \pm 2.2 \pm 2.0$	5.2 ± 0.7
`NT2`	16.6 ± 0.6	$33.1 \pm 2.1 \pm 2.1$	1.9 ± 0.5
all	76.7 ± 0.5		27.9 ± 1.6

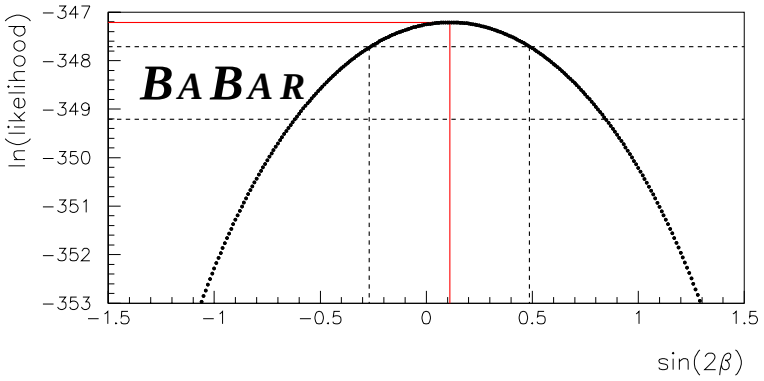

Figure 6: Variation of the log likelihood as a function of sin2β. The two horizontal dashed lines indicate changes in the log likelihood corresponding to one and two statistical standard deviations.

lepton categories have the lowest mistag fractions, but also have a low efficiency. The `Kaon` category, despite having a larger mistag fraction (19.7%), has a higher effective tagging efficiency; one-third of events are assigned to this category. Altogether, lepton and kaon categories have an effective tagging efficiency $Q \sim 20.8\%$. The neural network categories increase the effective tagging efficiency by $\sim 7\%$ to an overall $Q = (27.9 \pm 0.5)\%$ (statistical error only).

Of the 168 *CP* candidates, 120 are tagged: 70 as B^0 and 50 as $\overline{B}^0$. The number of tagged events per category is given in Table 7.

4.4 Results

The maximum-likelihood fit for sin2β, using the full tagged sample of $B^0/\overline{B}^0 \to J/\psi K^0_S$ and $B^0/\overline{B}^0 \to \psi(2S)K^0_S$ events, gives:

$$\sin 2\beta = 0.12 \pm 0.37(\text{stat}) \pm 0.09(\text{syst})\,. \tag{9}$$

For this result, the B^0 lifetime and Δm_d are fixed to the current best values [7], and Δt resolution parameters and the mistag rates are fixed to the values obtained from data as summarized in Tables 6 and 8. The log likelihood is shown as a function of sin2β in Figure 6.

The results of the fit for each type of *CP* sample and for each tagging category are given in Table 9. The contributions to the systematic uncertainty are summarized in Table 10.

Table 9: Result of fitting for *CP* asymmetries in the entire *CP* sample and in various subsamples.

sample	sin2β
CP sample	**0.12±0.37**
$J/\psi K^0_S$ ($K^0_S \to \pi^+\pi^-$) events	-0.10 ± 0.42
other *CP* events	0.87 ± 0.81
`Lepton`	1.6 ± 1.0
`Kaon`	0.14 ± 0.47
`NT1`	-0.59 ± 0.87
`NT2`	-0.96 ± 1.30

Table 10: Summary of systematic uncertainties. The different contributions to the systematic error are added in quadrature.

Source of uncertainty	Error on sin2β
τ^0_B	0.002
Δm_d	0.015
Δz resolution	0.019
time-resolution bias	0.047
measurement of mistag fractions	0.053
different mistag fractions	
for *CP* and non-*CP* samples	0.050
for B^0 and $\overline{B}^0$	0.005
background	0.015
total systematic error	**0.091**

Table 11: Results of fitting for apparent *CP* asymmetries in various charged or neutral flavor-eigenstate B samples.

Sample	Apparent *CP*-asymmetry
Hadronic charged B decays	0.03 ± 0.07
Hadronic neutral B decays	-0.01 ± 0.08
$J/\psi K^+$	0.13 ± 0.14
$J/\psi K^{*0}$ $(K^{*0} \to K^+\pi^-)$	0.49 ± 0.26

We estimate the probability of obtaining the observed value of the statistical uncertainty, 0.37, on our measurement of sin2β by generating a large number of toy Monte Carlo experiments with the same number of tagged *CP* events, and distributed in the same tagging categories, as in the *CP* sample in the data. We find that the errors are distributed around 0.32 with a standard deviation of 0.03, and that the probability of obtaining a value of the statistical error larger than the one we observe is 5%. Based on a large number of full Monte Carlo simulated experiments with the same number of events as our data sample, we estimate that the probability of finding a lower value of the likelihood than our observed value is 20%.

To validate the analysis we use the charmonium control sample, composed of $B^+ \to J/\psi K^+$ events and events with self-tagged $J/\psi K^{*0}$ $(K^{*0} \to K^+\pi^-)$ neutral B's. We also use the event samples with fully-reconstructed candidates in charged or neutral hadronic modes. These samples should exhibit no time-dependent asymmetry. In order to investigate this experimentally, we define an "apparent *CP* asymmetry", analogous to sin2β in Eq. 1, which we extract from the data using an identical maximum-likelihood procedure.

The events in the control samples are flavor eigenstates and not *CP* eigenstates. They are used for testing the fitting procedure with the same tagging algorithm as for the *CP* sample and, in the case of the B^+ modes, with self-tagging based on their charge. We also perform the fits for B^0 and $\overline{B}^0$ (or B^+ and B^-) events separately to study possible flavor-dependent systematic effects. For the charged B modes, we use mistag fractions measured from the sample of hadronic charged B decays.

In all fits, including the fits to charged samples, we fix the lifetime τ_{B^0} and the oscillation frequency Δm_d to the PDG values [7]. The results of a series of validation checks on the control samples are summarized in Table 11. The two high-statistics samples and the $J/\psi K^+$ sample give an apparent *CP* asymmetry consistent with zero. The 1.9σ asymmetry in the $J/\psi K^{*0}$ is interpreted as a statistical fluctuation.

Other *BABAR* time-dependent analyses presented at this Conference demonstrate the validity of the novel technique developed for use at an asymmetric B Factory. In particular, the measurement of the B^0-$\overline{B}^0$ oscillation frequency described in [10] uses the same time resolution function and tagging algorithm as the *CP* analysis, and the B^0 lifetime measurement described in [11] uses the same inclusive vertex reconstruction technique as the *CP* analysis. Both result are consistent with the world average [7].

4.5 Current knowledge of the angle β

Figure 7 shows the $(\bar{\rho}, \bar{\eta})$ plane, with *BABAR*'s measured central value of sin2β shown as two straight lines. There is a two-fold ambiguity in deriving a value of β from a measurement of sin2β. Both choices are shown with cross-hatched regions corresponding to 1σ and 2σ experimental

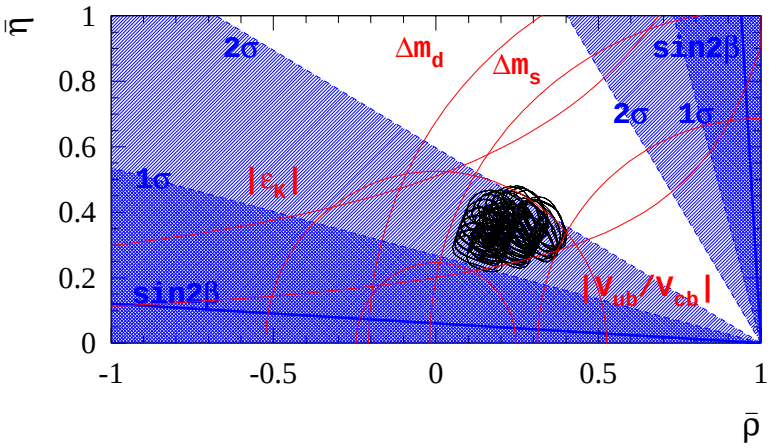

Figure 7: Present constraints on the position of the apex of the Unitarity Triangle in the $(\bar{\rho}, \bar{\eta})$ plane. Our result $\sin 2\beta = 0.12 \pm 0.37(\text{stat})$ is represented by cross-hatched regions corresponding to one and two statistical standard deviations. The fitting procedure is described in Ref. [12].

uncertainty. The ellipses correspond to the regions allowed by all other measurements that constrain the Unitarity Triangle for a variety of representative theoretical parameters. This procedure is discussed in detail in [12]. The following set of measurements and model-dependent parameters are used: $|V_{cb}| = 0.0402 \pm 0.017$; $|V_{ub}/V_{cb}| = \langle |V_{ub}/V_{cb}| \rangle \pm 0.0079$; $\Delta m_d = 0.472 \pm 0.017\,\hbar\,\text{ps}^{-1}$; $|\epsilon_K| = (2.271 \pm 0.017) \times 10^{-3}$; the set of amplitudes corresponding to a 95%CL limit of $14.6\,\hbar\,\text{ps}^{-1}$ for Δm_s; $\langle |V_{ub}/V_{cb}| \rangle$ in [0.070, 0.100]; B_K in [0.720, 0.980]; $f_{B_d}\sqrt{B_{B_d}}$ in [185, 255] MeV; and ξ_s in [1.07, 1.21].

In Figure 8, a summary of all existing direct measurements of $\sin 2\beta$ is reported. The PDG 2000 world average, obtained from the OPAL [13] and CDF [14] results, is compared with a new average that includes the recent ALEPH [15], Belle [16] and BABAR [9] results. The new measurements from the two B factories improved the knowledge of $\sin 2\beta$ by a factor 2.

5 Study of B $\to$ charmless 2-body decays

5.1 Interest of the measurement

The branching fractions for the rare charmless decays $B^0 \to h^+h^-$ $(h = \pi, K)$ provide important information in the study of *CP* violation. If the tree level diagram dominates the decay, the $\pi^+\pi^-$ decay mode can be used to extract the angle α of the Unitarity Triangle. If the penguin contribution is not negligible, large theoretical uncertainties [17] complicate the analysis and the extraction of α will require a full isospin analysis [18]. On the other hand, large penguin amplitude improves the prospects for observing direct *CP* violation as an asymmetry in the decay rates for $B^0 \to K^+\pi^-$ and $\overline{B}^0 \to K^-\pi^+$.

The decay $B^0 \to K^+\pi^-$ is dominated by the $b \to sg$ penguin amplitude, and provides an estimate of the scale of penguin pollution in the $\pi^+\pi^-$ decay. Precise measurement of the decay rates for $\pi\pi$ and $K\pi$ decays is therefore of central importance.

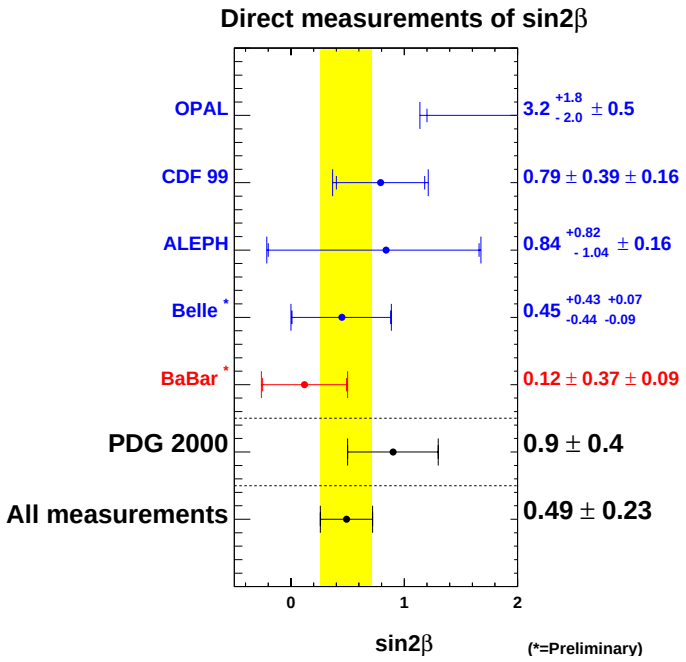

Figure 8: Existing direct measurements of $\sin 2\beta$. The input measurements are in Refs. [13], [14], [15], [16], [9].

5.2 Analysis strategy

The first step of this analysis consists in selecting decays B $\to h^+h^-$, where $h^\pm$ is either a pion or a kaon. B decays to charm mesons are not a significant background to charmless two-body decays because of the relatively small CM momenta of decay products produced from the $b \to c$ transition. The background is dominated by the continuum production of light quarks, $e^+e^- \to q\overline{q}$ $(q = u, d, s, c)$, which typically exhibits a two-jet structure in the CM frame. The topology is markedly different from that of real $B \to h^+h^-$ events, which is more spherically symmetric. This difference is exploited using the angle θ_S between the sphericity axes, evaluated in the CM frame, of the B candidate and the remaining charged and neutral particles in the event.

Further separation between signal and continuum background is provided by a Fisher discriminant technique [19]. The Fisher discriminant $\mathcal{F}$ is calculated from a linear combination of 9 discriminating variables constructed from the scalar sum of the momenta of all charged and neutral particles (excluding the candidate daughter tracks) flowing into 9 concentric cones centered on the B-candidate thrust axis in the CM frame. More energy will be found in the cones nearer the candidate thrust axis in jet-like continuum background events than in the more isotropic $B\overline{B}$ events.

Once the decay $B \to h^+h^-$ is identified, the separation between different channels is obtained using two different approaches:

- likelihood analysis, in which the K-π separation is determined on a statistical basis;
- cut based analysis, in which the K-π separation is performed track-by-track.

A good understanding of the particle identification performances is essential in both analyses.

Table 12: Summary of $B \to$ two-body branching fraction results. Shown are the central fit values N_S, the statistical significance, and the measured branching fractions $\mathcal{B}$. For the KK mode, the 90% confidence level upper limits are given. The first errors are statistical and the second systematic.

Mode	N_S	Stat. Sig.	$\mathcal{B}\,(10^{-6})$
$\pi^+\pi^-$	29^{+8+3}_{-7-4}	5.7σ	$9.3^{+2.6+1.2}_{-2.3-1.4}$
$K^+\pi^-$	38^{+9+3}_{-8-5}	6.7σ	$12.5^{+3.0+1.3}_{-2.6-1.7}$
K^+K^-	7^{+5}_{-4} (< 15)	2.1σ	< 6.6

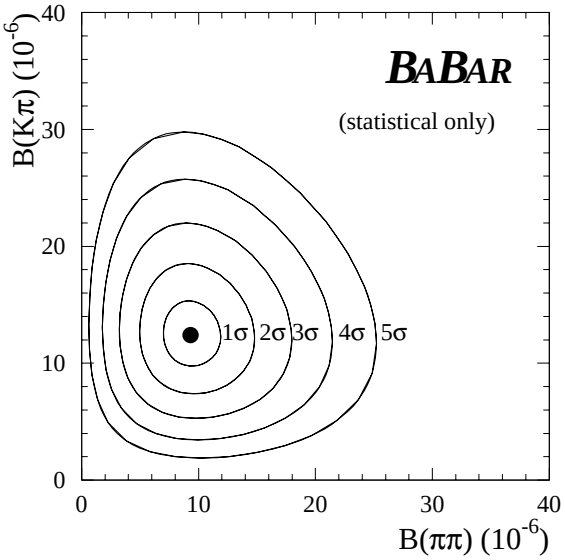

Figure 9: The central value (filled circle) for $\mathcal{B}(B^0 \to \pi^+\pi^-)$ and $\mathcal{B}(B^0 \to K^+\pi^-)$ along with the $n\sigma$ statistical contour curves for the global likelihood fit, where $n\sigma$ corresponds to a change of n^2 in $-2\log\mathcal{L}$.

5.3 Results

We determine branching fractions for $\pi^+\pi^-$ and $K^+\pi^-$ decays and an upper limit for the K^+K^- decay using the results of the global likelihood fit. The results are summarized in Table 12. For the KK mode we calculate the 90% confidence level upper limit yield and decrease the efficiency by the total systematic error (24%) before calculating the upper limit branching fraction. The statistical significance of a given signal yield is determined by setting the yield to zero and maximizing the likelihood with respect to the remaining variables.

Figure 9 shows the $n\sigma$ likelihood contour curves, where σ represents the statistical uncertainty only. The curves are computed by maximizing the likelihood with respect to the remaining variables in the fit.

6 Summary

PEP-II and BABAR had a beautiful start. In their first year of data taking, they have reached about 85% of the design peak luminosity, exceeded the design daily luminosity and accumulated almost 20 fb^{-1} on tape.

The first physics results, based on about 8 fb^{-1}, have been produced. This talk reviews the first results obtained by BABAR in the measurement of $\sin 2\beta$ and in the studies of $B \to$ charmonium and $B \to$ two body charmless decays.

The results for the data collected in the entire first run of data taking (about 24 fb^{-1}) is expected to be available in Spring 2001.

Acknowledgments

The work presented in this report was supported by the Department of Energy contract DE-AC03-76SF00515.

References

[1] M.H. Schune, *Physics results from* BABAR *and prospects*, these proceedings.

[2] BABAR *Technical Design Report*, BABAR Collaboration, D. Boutigny *et al.*, SLAC-R-457, March 1995.

[3] *The* BABAR *Physics Book: Physics at an Asymmetric B Factory*, BABAR Collaboration, P.F. Harrison, ed. *et al.*, SLAC-R-504, October 1998.

[4] BABAR Collaboration, B. Aubert *et al.*, SLAC-PUB-8539, July 2000.

[5] BABAR Collaboration, B. Aubert *et al.*, hep-ex/0008049.

[6] BABAR Collaboration, B. Aubert *et al.*, hep-ex/0008050.

[7] Particle Data Group, D.E. Groom *et al.*, Eur. Phys. Jour. C **15**, 1 (2000).

[8] ARGUS Collaboration, H. Albrecht *et al.*, Phys. Lett. **B254** (1991) 288.

[9] BABAR Collaboration, B. Aubert *et al.*, hep-ex/0008048.

[10] BABAR Collaboration, B. Aubert *et al.*, hep-ex/0008052.

[11] BABAR Collaboration, B. Aubert *et al.*, hep-ex/0008060.

[12] See, for example, "Overall determinations of the CKM matrix", in [3] Section 14 and the references therein.

[13] OPAL Collaboration, K. Ackerstaff *et al.*, Eur. Phys. Jour. C **5**, 379 (1998).

[14] CDF Collaboration, T. Affolder *et al.*, Phys. Rev. **D61**, 072005 (2000).

[15] ALEPH Collaboration, R. Barate *et al.*, hep-ex/0009058.

[16] BELLE Collaboration, H. Aihara *et al.*, hep-ex/0010008.

[17] M. Gronau, Phys. Rev. Lett. **63**, 1451 (1989).

[18] M. Gronau, Phys. Rev. Lett. **65**, 3381 (1990).

[19] CLEO Collaboration, D.M. Asner *et al.*, Phys. Rev. **D53**, 1039 (1996).